CHEMISTRY
A EUROPEAN JOURNAL

FULL PAPER

DOI: 10.1002/chem.201201472

Water Oxidation with Molecularly Defined Iridium Complexes: Insights into Homogeneous Versus Heterogeneous Catalysis

Henrik Junge,[a] Nicolas Marquet,[a] Anja Kammer,[a] Stefania Denurra,[a, b] Matthias Bauer,*[c] Sebastian Wohlrab,[a] Felix Gärtner,[a] Marga-Martina Pohl,[a] Anke Spannenberg,[a] Serafino Gladiali,[a, b] and Matthias Beller*[a]

Abstract: Molecularly defined Ir complexes and different samples of supported IrO_2 nanoparticles have been tested and compared in the catalytic water oxidation with cerium ammonium nitrate (CAN) as the oxidant. By comparing the activity of nano-scaled supported IrO_2 particles to the one of organometallic complexes it is shown that the overall activity of the homogeneous Ir precursors is defined by both the formation of the homogeneous active species and its conversion to Ir^{IV}-oxo nanoparticles. In the first phase of the reaction the activity is dominated by the homogeneous active species. With increasing reaction time, the influence of nano-sized Ir-oxo particles becomes more evident. Notably, the different conversion rates of the homogeneous precursor into the active species as well as the conversion into Ir-oxo nanoparticles and the different particle sizes have a significant influence on the overall activity. In addition to the homogeneous systems, IrO_2@MCM-41 has also been synthesized, which contains stabilized nanoparticles of between 1 and 3 nm in size. This latter system shows a similar activity to $IrCl_3{\cdot}xH_2O$ and complexes **4** and **5**. Mechanistic insights were obtained by in situ X-ray absorption spectroscopy and scanning transmission electron microscopy.

Keywords: heterogeneous catalysis · homogeneous catalysis · iridium · nanoparticles · oxygen · water oxidation

Introduction

Photocatalytic water-splitting to oxygen and hydrogen with the help of sunlight is of significant interest for the development of more benign energy technologies.[1] When applying organometallic catalysts for this process most efforts have focused on hydrogen generation, because it is expected to play an important role as secondary energy carrier for energy supply and storage.[2] Whereas the reduction of protons to hydrogen, a two electron process, has been investigated with considerable success,[3] water oxidation to oxygen is more difficult, because it is endothermic ($E^0 = 1.23$ eV at pH 0.0) and four electrons have to be transferred to an electron acceptor per molecule of generated oxygen [Eq. (1)].[4]

$$2\,H_2O \longrightarrow O_2 + 4\,H^+ + 4\,e^- \qquad (1)$$

Unfortunately, so far only few semiconducting materials are able to perform overall water splitting.[5] Hence, to develop more efficient catalysts the overall process is typically separated into its two half reactions, water oxidation and water reduction, which are studied autonomously. In this respect, previous efforts to oxidize water with molecularly defined catalyst precursors mainly focused on ruthenium-based systems. Pioneering work has been performed by Meyer and co-workers,[6] followed by other groups.[4]

Recently, iridium complexes have been identified to be highly active water oxidation catalysts.[7] It is important to note that the majority of the catalyst systems applied so far for oxygen generation makes use of strong oxidants such as cerium ammonium nitrate (CAN), iodate (IO_3^-), peroxodisulfate ($S_2O_8^{2-}$), Co^{3+} ammonia compounds or $[Ru(bipy)_3]^{3+}$ (Scheme 1).[8–14] Nevertheless, recently ruthenium complexes allowed also for photocatalytically driven reactions.[15–17]

Apart from organometallic complexes also heterogeneous materials like RuO_2 and IrO_2 are known to oxidize water in the presence of sacrificial oxidants.[18] Therefore, it is interesting to get more insights into the real catalyst species. To distinguish between an active homogeneous or heterogeneous catalyst, different methods such as kinetic isotope effect

---

[a] Dr. H. Junge, Dr. N. Marquet, A. Kammer, S. Denurra,
Dr. S. Wohlrab, F. Gärtner, Dr. M.-M. Pohl, Dr. A. Spannenberg,
Prof. Dr. S. Gladiali, Prof. Dr. M. Beller
Leibniz-Institut für Katalyse e.V.
Albert-Einstein-Straße 29a, 18059 Rostock (Germany)
Fax: (+49) 381-1281-5000
E-mail: matthias.beller@catalysis.de

[b] S. Denurra, Prof. Dr. S. Gladiali
Università di Sassari
Dipartimento di Chimica e Farmacia,
Via Vienna 2, 07100 Sassari (Italy)

[c] Prof. Dr. M. Bauer
Technische Universität Kaiserslautern
Fachbereich Chemie,
Erwin-Schrödinger-Straße 54
67663 Kaiserslautern (Germany)
E-mail: bauer@chemie.uni-kl.de

Supporting information for this article is available on the WWW under http://dx.doi.org/10.1002/chem.201201472.

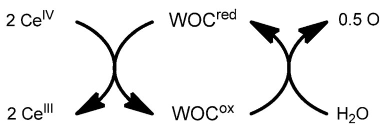

Scheme 1. Water oxidation in a two component system with Ce^{IV} as sacrificial oxidant. WOC = water oxidation catalyst.

investigations, UV/Vis, TEM, powder X-ray diffraction, XPS, analytical thermogravimetry/differential thermal analysis (TG/DTA) measurements, or an electrochemical quartz crystal nanobalance (EQCN) have been used.[7c,8a,19–21] For example, it has been observed by Crabtree that kinetic isotope effects[8a] differ when soluble iridium catalysts or IrO_x nanoparticles are used. In addition, the deposition of measurable amounts of the soluble catalysts on electrodes on short timescales (minutes) was reported.[20]

In our previous work, we demonstrated that simple $IrCl_3{\cdot}xH_2O$ and $Ir(acac)_3$ (iridiumacetylacetonate) constitute highly efficient catalysts for water oxidation. By using $IrCl_3{\cdot}xH_2O$, we were able to detect Ir-containing nanoparticles in the reaction mixture with sizes of <2 nm in a ceria matrix by using high-angle annular dark field scanning transmission electron microscopy (HAADF-STEM) combined with EDX.[22] Similar results were reported by Grotjahn for molecularly defined Ir complexes.[19] In addition, the degradation of the iridium compounds has been investigated in different organic solvents by NMR measurements.[14,19] These observations prompted us to focus further on whether the metal precursors lead to molecularly defined species or nm-sized particles as active catalysts for water oxidation. In this paper, we present efficient water oxidation catalysis with both Ir complexes as well as nano-scaled IrO_2 particles. To characterize the active catalysts in situ, X-ray absorption near edge structure (XANES) and extended X-ray absorption fine structure (EXAFS) measurements, as well as scanning transmission electron microscopy (STEM) investigations were performed.

Results and Discussion

At the start of this work, the Ir-phenylazole complexes **1–5** (Figure 1) were tested as pre-catalysts in the water oxidation half reaction to generate molecular oxygen. These complexes are available based on our experience in the synthesis of new Ir-based photosensitizers for the photocatalytic hydrogen generation from water.[23] The chloro-bridged dimers $[\{(C\^{}N)_2Ir(\mu\text{-}Cl)\}_2]$ can be synthesized through various protocols,[24] however we have chosen the previously described procedure, shown in Figure 1 (top), in which **1–5** are accessible by direct cyclometalation of $IrCl_3{\cdot}xH_2O$ with the respective HC^N ligands.[23] This is a convenient approach to obtain the desired product without the necessity of purification steps. The corresponding 2-phenylazole ligands are commercially available. In a typical experiment, Ir (1 µmol) (i.e., 0.5 µmol of the dimeric complex) was used as the catalyst in water (10 mL) containing Ce^{IV} (CAN) (1700 µmol) as the sacrificial oxidant. The evolved gas was quantitatively measured by using an automatic gas burette[25] and analyzed by GC. In fact, all of the complexes showed significant activities and the conversion was in between 92 and 98 % with respect to the oxidant CAN and provided approximately 10 mL of oxygen. The experiments are summarized in Table 1. For comparison, results for $Ir(acac)_3$ and $IrCl_3{\cdot}xH_2O$ have also been included.

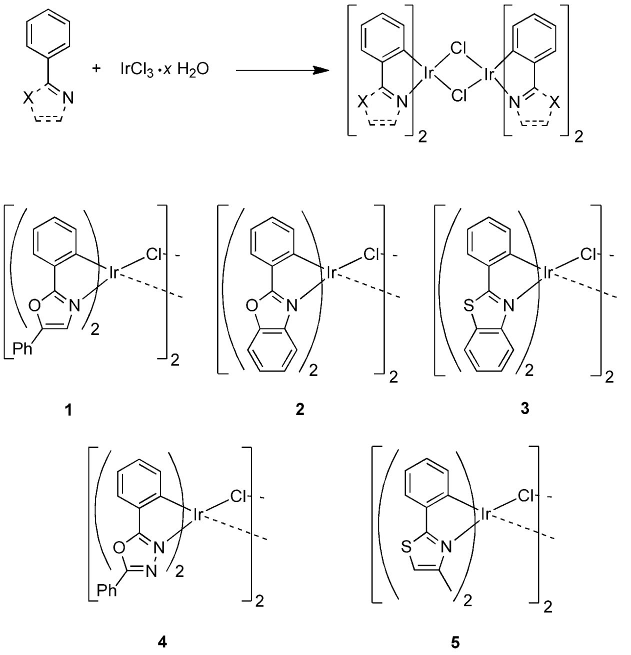

Figure 1. Synthesis of chloro-bridged dimers $[\{(C\^{}N)_2Ir(\mu\text{-}Cl)\}_2]$ **1–5**.

Table 1. Oxygen evolution rates for the molecularly defined water oxidation catalyst precursors using Ce^{IV} as oxidant.

Entry[a]	Catalyst precursor	[Ir] amount [µmol]	TOF $[h^{-1}]$[b,c]	TOF_{max} $[h^{-1}]$[b,d]	Ref.
1	$Ir(acac)_3$	1.08	755	1177	[22]
2	$IrCl_3{\cdot}xH_2O$	1.04	161	303	[22]
3	**1**	1.06	570	966	this paper
4	**2**	1.04	103	364	this paper
5	**3**	1.01	79	317	this paper
6	**4**	1.10	170	463	this paper
7	**5**	1.08	188	498	this paper
8	**6**	1.04	313	735	this paper
9	**7**	1.04	276	604	this paper

[a] General conditions: H_2O (10 mL), CAN (1700 µmol), ca. 1 µmol cat., 25 °C, dark. [b] TOF values are given in $mol(O_2){\cdot}mol(Ir)^{-1}\,h^{-1}$. [c] TOF was calculated as an average TOF between 0 % and 85–89 % of CAN conversion for entries 1 and 2 and between 0 and 73–82 % of CAN conversion for entries 3 to 9. After that, the kinetics drop due to the depletion of Ce^{IV} concentration. [d] TOF_{max} has been defined as the highest observed TOF during the reaction by graphical display of TOF versus time (see, for example, the Supporting Information, SI6-3 to SI6-6). The reproducibility is in the range of 1–15 %.

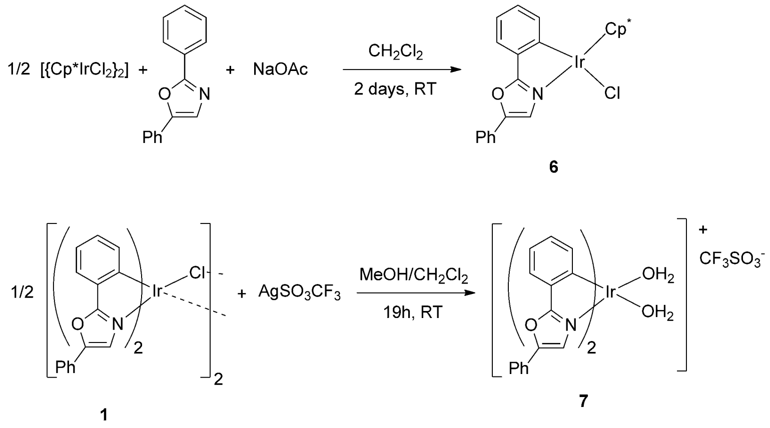

Figure 2. Synthesis of monomeric water oxidation catalysts **6** and **7**.

Among all of the chloro-bridged dimers [{(C^N)$_2$Ir(μ-Cl)}$_2$] **1**–**5**, complex **1** showed the highest activity (Table 1, entry 3), which is only slightly less than the activity of Ir(acac)$_3$ (Table 1, entry 1). Whereas when using **4** and **5** (Table 1, entries 6 and 7), approximately one third of the overall activity and half of the TOF$_{max}$ were achieved. Noteworthy, the Ir precursors **2** and **3** gave lower TOF values (Table 1, entries 4 and 5). In addition, from the most promising ligand 2,5-diphenyloxazole (2,5-dpo), the complexes [Cp*Ir(2,5-dpo)Cl] (**6**) and [Ir(2,5-dpo)$_2$(H_2O)$_2$]CF_3SO_3 (**7**) (Figure 2) were synthesized. The syntheses have been performed according to the reported procedures of the analogue phenylpyridine (ppy) derivatives starting either from the dimeric iridium Cp*-chloro complex and the 2,5-dpo ligand or from **1**, respectively (Figure 2).[8b,26,27] In the case of [Cp*Ir(2,5-dpo)Cl] (**6**), crystals suitable for X-ray crystal structure analysis were obtained from a CH_2Cl_2/hexane mixture.[28] Detailed information for the structure is provided in the Supporting Information (Figure S2-1). The analytical data of the new compounds **5**,[29] **6**, and **7** (^{1}H and ^{13}C NMR, IR spectroscopy and MS spectrometry are listed in the Experimental Section). Both of the Ir complexes **6** and **7** were more active than **2**–**5**, but less active than **1** (Table 1, entries 8 and 9).

Next, we were interested to determine if the iridium oxide nanoparticles were formed during the water oxidation applying the dimeric Ir species. Therefore, typical reaction mixtures from the catalytic experiments containing **1** and **4**, $IrCl_3$•$x$$H_2O$, and Ir(acac)$_3$ as well as commercially available IrO_2 were investigated in more detail by X-ray absorption spectroscopy (XAS) measurements. Whereas the XANES part of XAS is mainly sensitive to the oxidation state of an X-ray-absorbing atom by the shape and position of the white line (first resonance after the edge jump), the EXAFS (extended X-ray absorption fine structure) part yields type, number, and distance of coordinating atoms to the X-ray absorber.[30–33]

Figure 3 shows the XANES spectra at the Ir L$_3$-edge of the pre-catalysts IrO_2, $IrCl_3$•$x$$H_2O$, Ir(acac)$_3$, **1** and **4** in comparison to the spectra under water oxidation conditions. The corresponding EXAFS spectra are given in Figure 4. The structural parameters obtained by fitting these spectra with theoretical models are summarized in Table 2. In general, there are two indicators of the oxidation state in the XANES spectra. The first is the intensity of the so-called white-line (sharp resonance after the edge rise), which gains intensity with increasing oxidation state[30] due to the increasing number of final states of the p→d transition. The second is the weaker signal after the white line, which is

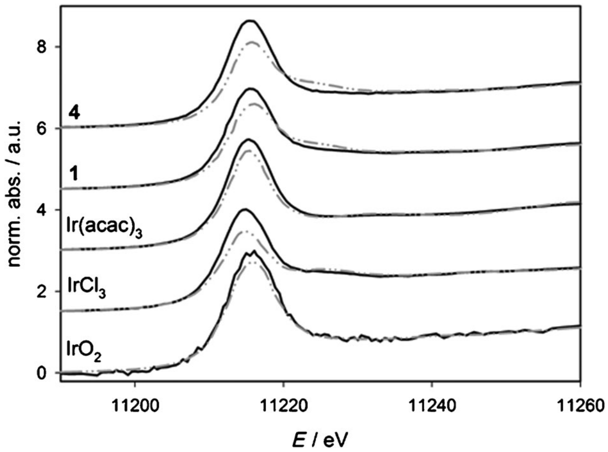

Figure 3. XANES spectra of the pre-catalysts (gray dotted dashed line) IrO_2, $IrCl_3$•$x$$H_2O$, Ir(acac)$_2$, **1**, **4** and the corresponding spectra recorded in course of water oxidation reactions (black line).

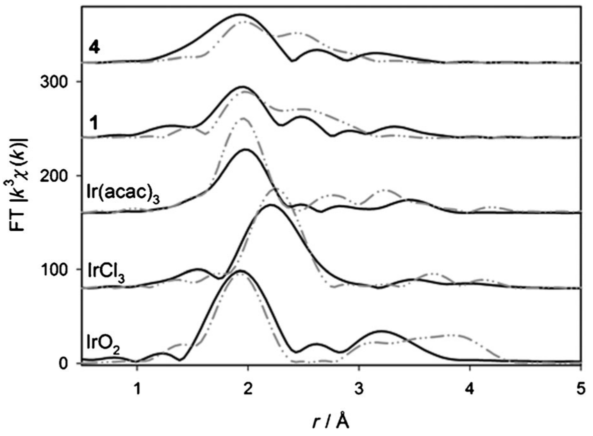

Figure 4. Fourier-transformed EXAFS spectra of the pre-catalysts (gray dotted dashed line) IrO_2, $IrCl_3$•$x$$H_2O$, Ir(acac)$_2$, **1**, **4** and the corresponding spectra recorded in course of water oxidation reactions (black line).

Table 2. Results of fitting the experimental EXAFS data with theoretical models. The average values from the LC-XANES fit for oxidation state determination are also given.

Sample	Abs-Bs	N(Bs)	R(Abs-Bs) [Å]	σ(Abs-Bs) [Å^{-2}]	LC-XANES fit IrO$_2$/Precatalyst[b]
IrO$_2$	Ir–O	6.9 ± 0.7	1.99 ± 0.02	0.008 ± 0.001	
	Ir–Ir	3.1 ± 0.3	3.15 ± 0.04	0.013 ± 0.001	
	Ir–Ir	2.5 ± 0.3	3.54 ± 0.04	0.005 ± 0.001	
IrO$_2$ WOC	Ir–O	6.1 ± 0.6	1.99 ± 0.02	0.003 ± 0.001	
	Ir–Ir	1.4 ± 0.1	3.14 ± 0.04	0.002 ± 0.001	
IrCl$_3$·xH$_2$O	Ir–O	3.0 ± 0.3	2.18 ± 0.02	0.009 ± 0.001	
	Ir–Cl	3.0 ± 0.3	2.36 ± 0.02	0.005 ± 0.001	
	Ir–Ir	1.1 ± 0.1	3.50 ± 0.03	0.009 ± 0.001	
IrCl$_3$·xH$_2$O WOC	Ir–O	3.4 ± 0.3	2.16 ± 0.02	0.002 ± 0.001	≈28.5/71.5 %
	Ir–Cl	2.3 ± 0.2	2.40 ± 0.02	0.004 ± 0.001	
Ir(acac)$_3$	Ir–O	6[a]	2.01 ± 0.02	0.006 ± 0.001	
	Ir-C	6[a]	2.93 ± 0.03	0.013 ± 0.001	
	Ir–C	3[a]	3.19 ± 0.03	0.002 ± 0.001	
Ir(acac)$_3$ WOC	Ir–O	6.1 ± 0.6	2.04 ± 0.02	0.011 ± 0.001	≈41/59 %
	Ir–C	4.1 ± 0.4	3.01 ± 0.03	0.015 ± 0.002	
	Ir–Ir	1.3 ± 0.1	3.36 ± 0.03	0.012 ± 0.001	
1	Ir–C/N[c]	4[a]	2.00 ± 0.02	0.039 ± 0.004	
	Ir–Cl	2[a]	2.36 ± 0.02	0.112 ± 0.011	
	Ir–C	4[a]	2.39 ± 0.02	0.039 ± 0.004	
	Ir–C	6.1 ± 1.2	2.80 ± 0.03	0.081 ± 0.016	
1 WOC	Ir–O/C[c]	5.6 ± 0.6	2.02 ± 0.02	0.084 ± 0.005	≈52/48 %
	Ir–Cl	0.8 ± 0.1	2.48 ± 0.02	0.032 ± 0.003	
	Ir–Ir	0.5 ± 0.2	3.24 ± 0.03	0.032 ± 0.006	
4	Ir–C/N[c]	4[a]	2.01 ± 0.02	0.005 ± 0.001	
	Ir–Cl	2[a]	2.35 ± 0.02	0.025 ± 0.003	
	Ir–C	4[a]	2.37 ± 0.02	0.004 ± 0.001	
	Ir–C	6.1 ± 1.2	2.80 ± 0.03	0.081 ± 0.016	
4 WOC	Ir–O/C[c]	6.7 ± 0.6	2.04 ± 0.02	0.018 ± 0.005	≈82/18 %
	Ir–Cl	0.4 ± 0.1	2.56 ± 0.02	0.002 ± 0.003	
	Ir–Ir	1.6 ± 0.2	3.28 ± 0.03	0.025 ± 0.006	

[a] Values were fixed to the expected value of the molecular/crystal structure. [b] Mean value of the obtained ranges given in the text are listed. [c] Carbon/nitrogen/oxygen cannot be distinguished as neighbors by EXAFS.

rather intense for Ir^0,[30] of lower intensity for Ir^{III}, and finally disappears for Ir^{IV}.[31] As can be seen in all the XANES spectra (Figure 3), the white line increases, whereas the second resonance, observed in all Ir^{III} pre-catalysts, is reduced in intensity during water oxidation reaction. A significant contribution of an Ir^{IV} species is therefore suspected in all spectra recorded under water oxidation conditions.

To quantify the amount of Ir^{III} and Ir^{IV} fractions in the spectra, a linear combination (LC) fit approach was used by fitting the WOC spectra with the pre-catalyst and IrO$_2$ reference spectra. Because the XANES white line is both affected by the oxidation state and the particle size,[32] this LC fit was not restricted to the area around the white line, as usually carried out. Instead, the second resonance was used as a unique fingerprint of the oxidation state and was fitted independently to circumvent particle size effects. The XANES spectra of solid IrO$_2$ and IrO$_2$ under reaction conditions showed only an intense white line at ≈11215 eV, and the second signal, which is indicative of oxidation states lower than Ir^{IV}, is missing. During water oxidation, the white line intensity is slightly increased. Since there is only Ir^{IV} present, this increase can be attributed to the formation of smaller particles compared to the solid pre-catalyst. This observation is also reflected in the results of the EXAFS analysis. For solid IrO$_2$ the crystal structure data[33] could be well reproduced within the error bar, with a sixfold nearest neighbor Ir–O contribution and an Ir–Ir shell with two atoms at 3.16 Å. The more distanced Ir–Ir shell could only be fitted with 2.5 Ir, which is due to particle size effects even in the reference. In contrast, under water oxidation conditions, a sixfold oxygen coordination is still found; however, the first Ir–Ir coordination is reduced by a factor of two, and the second Ir–Ir contribution is not detected anymore. This is in agreement with a reduced particle size of IrO$_2$ under water oxidation conditions.

The white line intensity of IrCl$_3$·xH$_2$O during the course of the reaction is significantly enhanced in comparison to the solid pre-catalyst IrCl$_3$·xH$_2$O. Examination of the second resonance at ≈11225 eV reveals still a contribution of IrCl$_3$·xH$_2$O. Thus, the white line increase can be due to oxidation state changes and particle size effects, as mentioned above. Fitting the spectrum of IrCl$_3$·xH$_2$O under water oxidation conditions by linear combination of IrCl$_3$·xH$_2$O and IrO$_2$ yields a composition of 68–75 % IrCl$_3$·xH$_2$O and 25–32 % IrO$_2$. The white line area and the second resonance were fit independently, resulting in a range of composition percentage. The EXAFS results given in Table 2 confirm this quantification. The first Ir–O contribution increases slightly compared to the solid pre-catalyst. In contrast, the Ir–Cl coordination number with 2.3 is reduced to around 75 % during the course of the reaction. Whereas with solid IrCl$_3$·xH$_2$O a third Ir–Ir shell can be fitted, but for the reaction mixture (due the low content of IrO$_2$) this is not possible.

Results for Ir(acac)$_3$ are similar to those of IrCl$_3$·xH$_2$O. Compared to the pre-catalyst the white line of Ir(acac)$_3$ in the reaction mixture is increased, and the second resonance showed a significant contribution of Ir^{III}. The linear combination fit of the spectra yields 55–63 % Ir(acac)$_3$ and 45–37 % IrO$_2$. Structural parameters achieved by fitting the experimental EXAFS spectra with theoretical models given in Table 2 are in good agreement with these results: The first Ir–O shell still contains six oxygen backscatterers, but the intensity of the first Ir–C contribution characteristic of Ir(acac)$_3$ is reduced to 4 atoms. This corresponds to 60 % Ir-

(acac)$_3$. The presence of IrO_2 is reflected in the third contribution consisting of 1.3 Ir atoms at a slightly increased distance compared with solid IrO_2.

By using complex **1**, a slightly smaller amount (44–52 %) of Ir^{III} is observed under water oxidation conditions in the LC-XANES fit, which corresponds to 48–56 % IrO_2. These results are also reflected in the EXAFS results of Table 2. The isolated complex **1** was fitted with good quality by using the molecular structure. Since carbon and nitrogen cannot be distinguished as backscatterers, they are summarized in one C/N shell. The characteristic structural features of **1** are the two chlorine neighbors per Ir center that follow from the dimeric structure shown in Figure 1. Moreover, a higher carbon shell consisting of more distanced atoms of the ligands is observed. In the reaction mixture slightly less than six atoms are found in the first coordination shell. Since the Ir–Cl contribution is still seen, the remaining **1** is supposed to be present in the reaction mixture. Thus, also coordinating carbon can be present in the first shell. As carbon and oxygen backscatterers cannot be distinguished, the nearest neighbor shell is labeled O/C in Table 2. Only 0.8 Cl are found in the Ir–Cl shell, indicating the presence of 40 % of **1**, which is in good agreement with the XANES results. Supposed that the third Ir–Ir shells originated only from IrO_2 species in the reaction mixture, the real Ir–Ir coordination number after de-averaging in the IrO_2 particles should be around 0.9. It is therefore slightly lower than in the other WOC reaction mixtures studied so far.

Investigating complex **4**, a further reduction of the Ir^{III} fraction under water oxidation conditions is observed. The LC fit results yield a composition of about 18 % Ir^{III} and 82 % Ir^{IV}. The EXAFS results, mainly the Ir–Cl shell support this ratio, since from the Ir–Cl coordination number of 0.4 a fraction of 20 % remaining **4** is calculated. However, the Ir–Ir shell showed a rather high coordination number of 1.6, according to a real coordination number in the IrO_2 particles of around 2. Therefore, larger particles of IrO_2 may be present in this reaction mixture. Having a closer look at the Ir–Ir coordination number in all WOC mixtures, a relative estimation of the IrO_2 particle sizes can be given: **4** ($N_{Ir-Ir} = 2 \pm 0.4$) > IrO_2 ($N_{Ir-Ir} = 1.4 \pm 0.3$) ≈ Ir(acac)$_3$ ($N_{Ir-Ir} = 1.3 \pm 0.3$) > **1**($N_{Ir-Ir} = 0.9 \pm 0.2$). It has to be mentioned, that in case of $IrCl_3 \cdot xH_2O$ the amount of formed IrO_2 is very small according to the LC-XANES analysis. The coordination number of the Ir–Ir shell in such a case can be easily below the detection limit of the EXAFS analysis.

All these findings are in general in good agreement with the results of TEM measurements. The HAADF-STEM images of Ir(acac)$_3$, $IrCl_3 \cdot xH_2O$, **1** and **4** have been taken after acting as precursors in the water oxidation reaction (Figure 5). To improve the chance to detect Ir nanoparticles, both, the concentration of Ir and the ratio of iridium to cerium have been increased ([Ir] (15 μmol) and CAN (3.4 mmol) in 50 mL water). After the reaction was finished, the solution has been concentrated to 10 mL. Thus, an influence of the modified reaction conditions onto the samples as well as a degradation of the Ir complexes after full consumption of CAN cannot be excluded. However, all samples have been treated in the same manner and therefore the differences should be significant. Starting from Ir(acac)$_3$, $IrCl_3 \cdot xH_2O$ and **1** (Figure 5 a-c and the Supporting Information, SI4-1-SI4-3) Ir-containing nanoparticles of 0.5 nm to 2 nm were detected. Whereas the Ir(acac)$_3$ sample contains predominantly particles in the range of 1 nm, smaller particles have been formed when starting from **1** (<1 nm). For $IrCl_3 \cdot xH_2O$, the size distribution is between approximately 0.5 and 2 nm.[22] These results are in agreement with the observations of Grotjahn, who detected Ir-containing nanoparticles with sizes between 2 and 10 nm.[19] On the other hand, starting from **4** (Figure 5 d and the Supporting Information SI4-4) no nanoparticles on the Ce matrix were detected, since these have obviously agglomerated to give bigger particles in the 10 μm range (Figure 5 e and the Supporting Information SI4-4).

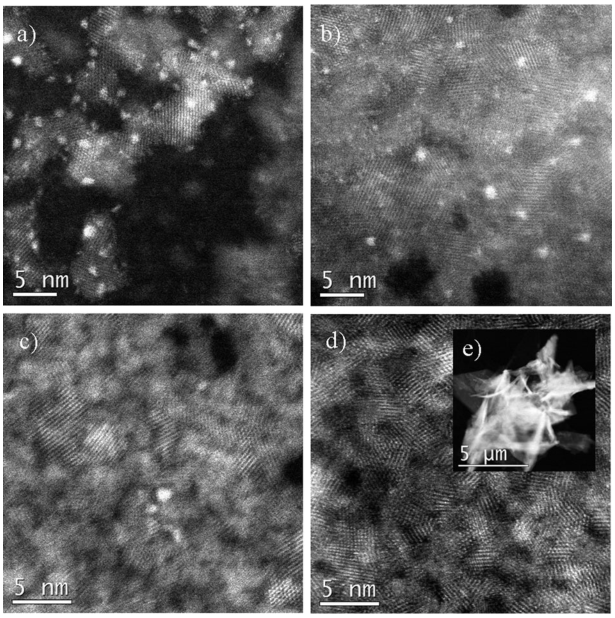

Figure 5. HAADF-STEM images of molecularly defined Ir complexes after the water oxidation reaction a) Ir(acac)$_3$, b) $IrCl_3 \cdot xH_2O$, c) **1**, d) **4**, inset e) Ir-containing particle.

Finally, we were interested in the activity of IrO_2 with respect to different particle sizes. Applying commercially available IrO_2, which consists of agglomerates of particles with a primary particle size of 1 to 3 nm (see the Supporting Information, Figure SI5-2), much less activity has been observed (Table 3, entry 1). In addition, three samples of isolated and stabilized IrO_2 particles on porous supports with sizes between 8 and 1 nm were synthesized. The applied nanoporous glasses (NPG)[34] and mesoporous silicas[35] are attractive catalyst supports to disperse catalysts and to limit particle growth in the order of their inherent pore size.[36] Their pore size distribution can be adjusted during the synthetic route. By applying these materials as supports for nanoparticles, effects such as particle ripening and leaching can be overcome. Additionally, highly and thermally stable surface areas of mesoporous silicas are favorable for a variety of oxide syntheses. Normally, the pore sizes of NPG's range from 10 to 1000 nm and pore volumes between 0.1 and 1.1 cm^3g^{-1} and inner surfaces up to 500 m^2g^{-1} are achieved. Much lower pore sizes and higher surface areas can be achieved with mesoporous silicas. These materials also possess surface areas up to more than 1000 m^2g^{-1}, whereas the pore sizes can be controlled and adjusted in the diameter range from 1.5 to more than 20 nm. For the synthesis of the supported IrO_2 samples, two NPG's (NPG-63 and NPG-27) and one mesoporous silica (MCM-41) have been chosen. The supported IrO_2 materials have been investigated in more detail by means of XRD and TEM. The XRD patterns of the samples IrO_2@NPG-63, IrO_2@NPG-27, IrO_2@MCM-41 and commercial IrO_2 are shown in the Supporting Information (Figure SI5-1) and compared with reported reflex positions for tetragonal iridium(IV) oxide. The phase purity and the nanocrystalline character of IrO_2 incorporated in NPG-63 and NPG-27 is clearly shown. Average crystallite sizes of 7.7 nm for IrO_2@NPG-63 and 7.3 nm for IrO_2@NPG-27 were estimated by using the Scherrer equation. The pore sizes of the glasses applied ($d_{pore} = 63/27$ nm) did not have a direct influence on the size of the IrO_2 crystallites formed within. Therefore, a smaller pore size of the silica support, like MCM-41 with $d_{pore} = 3.8$ nm, is required to influence the particle growth. The XRD pattern of IrO_2@MCM-41 showed no clear signals that could be assigned to the metal oxide.

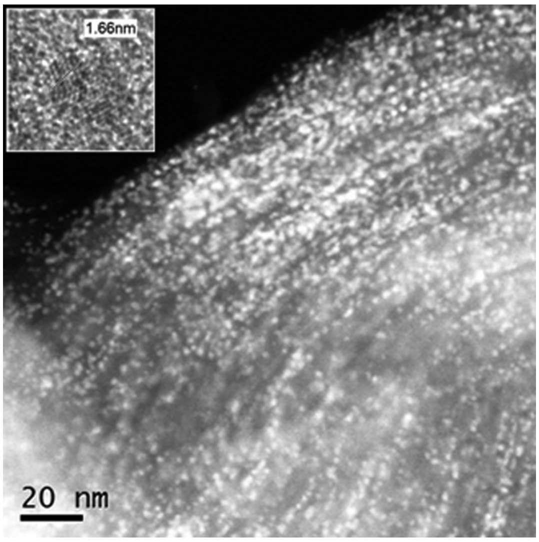

Figure 6. HAADF-TEM image of IrO_2@MCM-41; inset: high-resolution BF image of crystalline IrO_2 from IrO_2@MCM-41.

Table 3. Oxygen evolution rates for the IrO_2 nanoparticles using Ce^{IV} as oxidant.

Entry[a]	Catalyst precursor	[Ir] amount [μmol]	TOF $[h^{-1}]$[b,c]	TOF_{max} $[h^{-1}]$[b,d]	Ref.
1	IrO_2 (Strem)	1.28	35	347	[22]
2	4.8 % IrO_2@NPG-63	1.05	8.0	143	this paper
3	5.5 % IrO_2@NPG-27	1.27	18	238	this paper
4	9.3 % IrO_2@MCM-41	1.15	158	343	this paper

[a] General conditions: H_2O (10 mL), CAN (1700 μmol), IrO_2 (1 μmol), 25 °C, dark. [b] TOF values are given in $mol(O_2)\cdot mol(Ir)^{-1}\,h^{-1}$. [c] TOF was calculated between 0 and 85–89 % of CAN conversion for entry 1, 0 and 75 % of CAN conversion for entries 3 and 4. After that, the kinetics drop due to the depletion of Ce^{IV} concentration. The experiment in entry 2 has been stopped after 18 h at 30 % conversion. [d] TOF_{max} has been defined as the highest observed TOF during the reaction by graphical display of TOF versus time (see for example, the Supporting Information, SI6-1 and SI6-2). Reproducibility is in the range of 1–25 %, except for IrO_2@NPG-63 (30 %).

Further investigations by using TEM indicated the presence of highly dispersed and crystalline IrO_2 species in the mesoporous material; the sample IrO_2@MCM-41 showed a small apparent particle size between 1 and 3 nm and a crystalline structure (Figure 6).

The three synthesized IrO_2 samples were tested in the oxygen evolution reaction under the same conditions similar to the molecularly defined Ir complexes (Table 3). IrO_2@NPG-63 and IrO_2@NPG-27 with particle sizes of 7.7 nm and 7.3 nm, respectively, showed much less activity (Table 3, entries 2 and 3) than the commercially available IrO_2, which itself consists of aggregates of IrO_2 particles with primary particle sizes from 1 to 3 nm. Hence, an influence of the particle size on the activity is apparent. Interestingly, when IrO_2@MCM-41 is used with isolated and well-dispersed IrO_2 particles possessing sizes between 1 and 3 nm, much better activities are observed. Comparing the average TOF values with that of the homogeneous Ir-precursors, IrO_2@MCM-41 is equal to $IrCl_3{\cdot}xH_2O$ and may also compete with complexes **2**–**5**, although it is less active than **1** and $Ir(acac)_3$.

As a result of the various catalytic experiments and the mechanistic investigations, we conclude that the catalyst activity in this complex system is a result of both homogeneous and heterogeneous catalysis. Starting from stable coordinatively saturated Ir complexes, active homogeneous species as well as active nano-sized iridium-oxo species are formed. The latter nanoparticles can be furthermore converted into bulk iridium oxide and other deactivated species (Figure 7).

After an induction period, which lasts less than 10 min for **1** and $Ir(acac)_3$ and approximately 20 or 40 min for $IrCl_3{\cdot}xH_2O$ and **4**, respectively (see the Supporting Information, Figure SI6-3 to SI6-6), an increasing TOF is observed. Comparing the activities in this period, starting from homogeneous and heterogeneous catalyst precursors, it becomes obvious that the TOF_{max} values of up to 1200 h^{-1} should arise mainly from the active homogeneous Ir complexes, if no strong deleterious effects of supports are present. Therefore, the overall activity seems to be dominated by the active homogeneous species, which are formed by a rate according to k_1 (Figure 7). However, the generation of Ir^{IV}-oxo nanoparticles is expected to start already in this phase, probably after the generation of significant amounts of the active

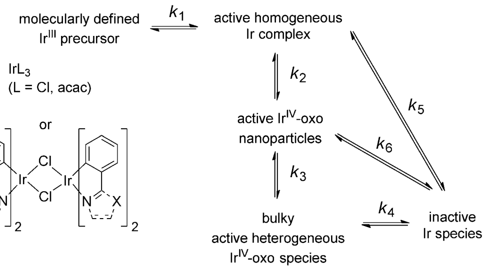

Figure 7. Hypothesis for the conversion of molecularly defined Ir complexes into Ir-O-species.

homogeneous species (k_2 in Figure 7). After 10–20 min for **1** and Ir(acac)$_3$ and approximately 90 min for **4** and 75 min for IrCl$_3$·xH$_2$O, respectively, the maximum TOF is reached. Its time and value are determined by the ratio of k_1 and k_2. At the peak TOF, the conversion of CAN has reached 30 to 50 %. Hence, the depletion of CAN as the reason for the activity decrease seems to be unlikely. This has been proven by an additional experiment with a higher amount of CAN and the same amount of **1**, which was allowed to react for seven days. In this experiment the highest TOF is also obtained within the first 20 min, when only 2 % of CAN has been consumed (see the Supporting Information, Figure SI6-7).

After having reached the maximum activity the TOF is more and more defined by the Ir^{IV}-oxo nanoparticles. Depending on k_2, there are significant differences in the extent of the conversion to the Ir^{IV}-oxo nanoparticles due to the different ligands in the Ir complexes. For example, after one hour Ir(acac)$_3$ and **1** were converted to Ir—O species with up to 40 and 50 %, respectively, whereas starting from **4** up to 82 % and starting from IrCl$_3$·xH$_2$O only 25 % Ir^{IV}-oxo nanoparticles have been generated within the same time. In the case of complexes with organic ligands, this conversion is accompanied by CO$_2$ generation due to a degradation of the ligands. In these cases the analysis of the gas phase after finishing the reactions resulted in significant contents of carbon dioxide, between 0.17 and 0.30 vol %. For **6**, an even higher CO$_2$ content has been observed (1.1 vol %), which is very likely due to the sensitivity of the Cp* ligand with respect to oxidative degradation; this has also been observed for other complexes.[21] During this phase of the major contribution of Ir—O species, the particle size of the formed iridium oxide nanoparticles is another important parameter influencing the activity. Whereas the highest activities for IrO$_2$ particles have been observed in the range of 1–3 nm, particles of more than 7 nm are significantly less active. Notably, the stabilization of such small nanoparticles on a porous support, as in the case of IrO$_2$@MCM-41, has a positive influence. At the end of the reaction the catalyst activity drops due to the depletion of CAN. Furthermore, during all phases, an agglomeration to bigger particles (k_3 in Figure 7) and a deactivation by the formation of inactive species (k_4, k_5, and k_6 in Figure 7) might occur.

Long-term catalyst tests revealed that the active species resulting from **1** can be used in longer term experiments of up to 11 days (see the Supporting Information, Figure SI7-1); they stay active after full conversion and addition of a new charge of CAN (Figure SI7-2). Thus, relatively high turnover numbers of 8139 and 7250, respectively, were achieved.

Finally, it is interesting to note that the Ir-oxo nanoparticles show a somewhat different behaviour during water oxidation. With IrO$_2$ by itself (as well as on supports), no induction period is observed, which is in agreement to a previous report.[19] The TOF is initially very high and then drops and remains quite stable until the depletion of CAN becomes evident, which leads to a further decrease (see the Supporting Information, Figure SI6-1 and SI6-2).

Conclusion

The activity of seven iridium complexes and different heterogeneous iridium oxide materials in the cerium-driven oxidation of water to oxygen has been compared. A combination of catalytic experiments, in situ X-ray absorption spectroscopy, XRD, and STEM measurements have shown that both molecular iridium species and Ir^{IV}-oxo nanoparticles are present in the water oxidation reactions. By applying organometallic precursors in the first phase of the reaction, the most active species are generated from the homogeneous precursors. During the course of the reaction nano-sized Ir-oxo species are formed that catalyze the water oxidation with lower activities, as it has been shown for preformed Ir^{IV}-oxo nanoparticles. However, this could at least in part be also an effect of the applied supports. The obtained catalyst activities of organometallic iridium complexes are a result of different conversion rates of the pre-catalyst into the active species as well as into Ir-oxo nanoparticles. Depending on the ligand, the particle size of the formed nanoparticles is different and has an important influence on the activity of the catalyst system. Thus, the tetrakis-(2,5-diphenyloxazole)-μ-(dichloro)diiridium(III) and Ir(acac)$_3$ belong to the most powerful systems studied here. Finally, IrO$_2$@MCM-41 with stabilized nanoparticles of comparable size (1–3 nm) has been prepared, which shows comparable activity to IrCl$_3$·xH$_2$O and complexes **4** and **5**.

Experimental Section

General protocol for the synthesis of tetrakis-(C^N)-μ-(dichloro)diiridium(III) 1–5: The cyclometalated iridium dimers were prepared by a procedure adapted from Bernhard et al.[14] in moderate yields. The ligands were purchased from commercial suppliers (Aldrich and Alfa Aesar). Stoichiometric quantities of the appropriate cyclometalating ligand (2.0 equiv, typically 1.0 mmol) were added to a mixture of iridium chloride (1.0 equiv, typically 0.5 mmol) in an ethoxyethanol/water mixture (3:1, 22 mL). The reaction mixture was heated under reflux (120 °C) with constant stirring for 24 h. The resulting precipitate was collected by suction filtration and washed with diethyl ether, and dried to yield the product [{(C^N)$_2$Ir-μ-Cl}$_2$]. With the exception of compound **5** (which is a new compound), compounds **1–4** are known already and the published analytical data correlate with our measured results.

Synthesis of tetrakis-(4-methyl-2-phenylthiazole)-μ-(dichloro)diiridium-(III) 5: *T*: 90 °C, *t* = 30 h. Orange solid. Yield: 36 %. ^{1}H NMR (300 MHz, CD_2Cl_2): $\delta = 7.47$ (4H, d, J(H,H) = 7.6 Hz), 7.00 (4H, bs), 6.81 (4H, t, J(H,H) = 7.4 Hz), 6.63 (4H, t, J(H,H) = 7.5 Hz), 6.20 (4H, d, J(H,H) = 7.3 Hz), 2.17 ppm (12H, s, CH_3); ^{13}C NMR (100 MHz, CD_2Cl_2): $\delta = 179.7$, 156.4, 142.9, 142.3, 133.3, 128.9, 124.1, 121.9, 112.2, 18.7 ppm; ATR-IR: $\tilde{\nu} = 3099$ (m), 3049 (w), 1579 (m), 1458 (m), 1282 (m), 1097 (m), 1024 (m), 759 (m), 731 (s), 720 cm^{-1} (s); MS (ESI-TOF/HRMS): *m*/*z*: calcd for $C_{20}H_{16}IrN_2S_2$: 541.038434; found: 541.03943 $[C_{20}H_{16}IrN_2S_2]^+$.

Synthesis of [Cp*Ir(2,5-diphenyloxazole)Cl] 6: Under an argon atmosphere, a slurry of [Cp*IrCl$_2$]$_2$ (370 μmol), 2,5-diphenyloxazole (767 μmol) and NaOAc (1.295 mmol) in CH_2Cl_2 (10 mL) was stirred at room temperature for 2 days and subsequently filtered over celite. The solvent was evaporated and the yellow solid was dried under vacuum. For purification, the solid was dissolved in CH_2Cl_2 (minimum amount) and filtered over celite. The solvent was removed under reduced pressure and the product dried under vacuum overnight to give a yellow solid. Yield: 74 %. ^{1}H NMR (300 MHz, CD_2Cl_2): $\delta = 7.81$ (1H, d, J(H,H) = 7.3 Hz), 7.76 (2H, d, J(H,H) = 6.8 Hz), 7.68 (1H, d, J(H,H) = 7.5 Hz), 7.53 (1H, s), 7.49 (2H, t, J(H,H) = 7.5 Hz), 7.40 (1H, t, J(H,H) = 7.3 Hz), 7.22 (1H, t, J(H,H) = 7.4 Hz), 7.09 (1H, t, J(H,H) = 7.4 Hz), 1.77 ppm (15H, s, H_{Cp}); ^{13}C NMR (75 MHz, CD_2Cl_2): $\delta = 174.9$, 162.6, 152.0, 136.6, 131.7, 130.8, 129.5, 129.4, 127.7, 124.4, 124.0, 122.5, 119.8, 88.3 (5C, Cp_{Ar}), 9.4 (Cp_{Me}) ppm; ATR-IR: $\tilde{\nu} = 3129$ (w), 2914 (w), 1597 (m), 1481 (m), 1393 (m), 1180 (m), 1051 (m), 765 (s), 731 (s), 718 (s), 705 cm^{-} (m); MS (ESI-TOF/HRMS): *m*/*z*: calcd for $C_{25}H_{25}IrNO$: 548.156556; found: 548.15735 $[M-Cl]^+$. The pure compound was obtained as orange crystals which turned to yellow when scratched for collection. Crystals suitable for X-ray diffraction were grown from a CH_2Cl_2/hexane mixture.

Synthesis of [Ir(2,5-diphenyloxazole)$_2$(H$_2$O)$_2$]CF$_3$SO$_3$ 7: Under an argon atmosphere, a solution of AgOTf in MeOH (10 mL) was added to a slurry of the dimer [(2,5-diphenyloxazole)$_2$Ir-(μ-Cl)]$_2$ in CH_2Cl_2 (10 mL). The reaction mixture was stirred overnight at room temperature. The solution was then filtered over celite and the filtrate was evaporated to yield a dark-orange oil. The oil was diluted with CH_2Cl_2 and hexane was added. Solvents were removed under reduced pressure and the product was obtained as a yellow solid which was dried under vacuum. Yield: 91 %; ^{1}H NMR (300 MHz, [D$_6$]DMSO): $\delta = 8.32$ (2H, s); 8.05 (4H, d, J(H,H) = 6.7 Hz); 7.74 (2H, d, J(H,H) = 7.0 Hz); 7.63 (4H, t, J(H,H) = 7.4 Hz); 7.55 (2H, t, J(H,H) = 7.3 Hz); 7.14 (2H, t, J(H,H) = 7.4 Hz); 7.08 (2H, t, J(H,H) = 7.4 Hz); 6.51 ppm (2H, d, J(H,H) = 7.3 Hz); ^{13}C NMR (75 MHz, [D$_6$]DMSO): $\delta = 172.8$, 151.7, 144.9, 131.9, 131.0, 129.9, 129.3, 128.6, 126.1, 124.9, 124.7, 124.6, 120.4 ppm; ATR-IR: $\tilde{\nu} = 3049$ (w), 1597 (m), 1491 (m), 1460 (m), 1208 (s), 1172 (s), 1041 (s), 1012 (s), 739 (m), 658 (m), 626 cm^{-} (s); MS (EI): *m*/*z*: calcd for $C_{15}H_{12}IrNO_2$: 431.5; found: 432 $[M-DPO-OTf-H_2O+H]^+$; *m*/*z*: calcd for $C_{30}H_{20}IrN_2O_2$: 632.7; found: 633 $[M-OTf-H_2O]^+$; *m*/*z*: calcd for $C_{31}H_{20}N_2O_5SF_3Ir$: 781.8; found: 782 $[M-2H_2O]^+$; MS (ESI-TOF/HRMS): *m*/*z*: calcd for $C_{30}H_{20}N_2O_2Ir$: 633.115; found: 633.1141, $[M-OTf-H_2O]^+$, *m*/*z*: calcd for CF_3O_3S: 148.95257; found: 148.95259, $[M]^+$.

Synthesis of supported IrO$_2$ on nanoporous silica or glasses: MCM-41 with a pore size of 3.8 nm was supplied by Süd-Chemie (Germany). Granulated nanoporous glasses specified by pore sizes of 27 nm (NPG-27) and 63 nm (NPG-63) were purchased from VitraBio GmbH (Steinach, Germany). The supports were characterized before usage with nitrogen adsorption using the five-point BET method and scanning and transmission electron microscopy. The syntheses of IrO_2 particles within these glasses were achieved by a process including an impregnation and calcination step. In the case of MCM-41, incipient wetness impregnation was applied to impregnate 800 mg of MCM-41 with 150 mg (0.369 mmol) H_2IrCl_6 dissolved in 1.5 mL water (IrO$_2$@MCM-41). Nanoporous glasses were impregnated in the same way by a solution of 106 mg (0.260 mmol) of H_2IrCl_6 dissolved in water (1.0 mL) for 1.0 g of NPG-27 (IrO$_2$@NPG-27) or a solution of 91 mg (0.224 mmol) of H_2IrCl_6 dissolved in water (1.3 mL) for 1.0 g NPG-63 (IrO$_2$@NPG-63). The concentrations of the chloride precursor were calculated according to the specific pore volumes and overall densities of the porous materials to ensure a comparable catalyst loading of all supports that was fixed at 9.3, 5.5 and 4.8 wt %, respectively. After completed incipient wetness impregnation the materials were dried at 60 °C. Afterwards the materials were calcined at 400 °C under air for 1 h using heating and cooling ramps of 5 °C min^{-1}. The calcined materials were washed three times with water and dried at 60 °C. The results of XRD and TEM are provided in the Supporting Information (SI5–1–3)

General procedure for oxygen evolution experiments: The catalytic experiments were carried out in an argon atmosphere and under the exclusion of air. Solvents were purified and degassed with standard procedures prior to use. Each experiment was performed in a glass reactor thermally equilibrated at 25 °C through a double mantle with a temperature-controlled circulating water bath. The reactor was always covered with aluminum foil during the reaction to exclude light effect.[22] The amount of evolved gases was quantitatively measured via an automatic gas burette[25] and qualitatively by GC (gas chromatograph HP7890N, carboxen 1000, TCD, external calibration). In a typical experiment, CAN (ca. 930 mg, 1.7 mmol) was introduced in the reactor that was than evacuated and filled with argon five times. Next, degassed and distilled water (10 mL) was added and the stirred solution was thermally equilibrated at 25 °C for several minutes. Then the catalyst (ca. 1 μmol [Ir]) was introduced in the reactor as a solid weighed in a Teflon crucible and gas evolution was recorded until the end of the reaction. After each reaction, a gas sample (ca. 5 mL) was taken and analyzed by gas chromatography (GC). All measured volumes have been corrected by the blank volume (0.7 mL). During the long term experiment the blank volume fluctuates between 0 and 1 mL.

X-ray absorption spectroscopy: X-ray absorption measurements were performed at the XAS beamline at the Ångströmquelle Karlsruhe (ANKA). The synchrotron beam current was between 80–140 mA at 2.5 GeV storage ring energy. A Si(111) double crystal monochromator was used for measurements at the Ir L3-edge (11.215 keV). The second monochromator crystal was tilted for optimal harmonic rejection. To perform operando studies, that is, under the original conditions, the spectra were recorded in fluorescence mode using a hyperpure Germanium detector with a cell that could be securated and filled under inert atmosphere. Measurements started 60 min after start of the reaction. In all cases stable spectral conditions were found after the acquisition of the first spectrum (30–60 min). Only in case of **4** evolving gas made the first spectra useless and stable conditions were found after 150 min. Measurements were carried out for 5–12 h, within that time window no changes in the spectra were detected. More details can be found in the Supporting Information.

TEM measurements: For the TEM measurements, samples of Ir(acac)$_3$, $IrCl_3{\cdot}xH_2O$, **1** and **4** were taken after acting as precursors in the water oxidation reaction, following the same protocol as described previously but with a higher concentration of Ir. The Ir precursor (15 μmol [Ir]) and CAN (3.4 mmol) were added to H_2O (50 mL). After completion of the reaction, the solution was concentrated to approximately 10 mL. The samples were then collected by depositing a drop of the pre-treated solution on a carbon-supported copper grid mesh 300. The TEM measurements were performed at 200 kV on a JEM-ARM200F (JEOL) that is aberration-corrected by a CESCOR (CEOS) for the scanning transmission (STEM) applications. The microscope is equipped with a JED-2300 (JEOL) energy-dispersive x-ray-spectrometer (EDXS) for chemical analysis. High-angle annular dark field (HAADF) and EDXS imaging were operated with spot size 5c and a 50 μm condenser aperture.

Acknowledgements

Parts of this work have been supported by the BMBF within the project "Light2Hydrogen" (Spitzenforschung und Innovation in den Neuen Ländern), by the Ministry for education, science and culture of Mecklenburg-Vorpommern and the European Union (Investing in our Future, European Regional Development) within the project "Nano4Hydrogen".

We thank P. Bartels, Ch. Fischer and A. Koch for their excellent analytical and technical support. F.G. thanks the Fonds der Chemischen Industrie (FCI) for a Kekulé grant. M.B. acknowledges the synchrotron ANKA (Karlsruhe, Germany) for provision of beamtime and the Carl-Zeiss foundation for financial support.

---

[1] a) H. Arakawa, M. Aresta, J. N. Armor, M. A. Barteau, E. J. Beckman, A. T. Bell, J. E. Bercaw, C. Creutz, E. Dinjus, D. A. Dixon, K. Domen, D. L. DuBois, J. Eckert, E. Fujita, D. H. Gibson, W. A. Goddard, D. W. Goodman, J. Keller, G. J. Kubas, H. H. Kung, J. E. Lyons, L. E. Manzer, T. J. Marks, K. Morokuma, K. M. Nicholas, R. Periana, L. Que, J. Rostrup-Nielson, W. M. H. Sachtler, L. D. Schmidt, A. Sen, G. A. Somorjai, P. C. Stair, B. R. Stults, W. Tumas, *Chem. Rev.* **2001**, *101*, 953–996; b) Q. Schiermeier, J. Tollefson, T. Scully, A. Witze, O. Morton, *Nature* **2008**, *454*, 816–823; c) N. S. Lewis, D. G. Nocera, *Proc. Natl. Acad. Sci. USA* **2006**, *103*, 15729–15735.

[2] a) J. A. Turner, *Science* **2004**, *305*, 972; b) N. Armaroli, V. Balzani, *Angew. Chem.* **2007**, *119*, 52–67; *Angew. Chem. Int. Ed.* **2007**, *46*, 52–66; c) L. Schlapbach, A. Züttel, *Nature* **2001**, *414*, 353–358.

[3] For reviews on light-driven water reduction systems, see: a) M. Wang, Y. Na, M. Gorlov, L. Sun, *Dalton Trans.* **2009**, 6458–6467; b) L. L. Tinker, N. D. McDaniel, S. Bernhard, *J. Mater. Chem.* **2009**, *19*, 3328–3337; c) E. D. Cline, S. Bernhard, *Chimia* **2009**, *63*, 709–713; d) T. S. Teets, D. G. Nocera, *Chem. Commun.* **2011**, *47*, 9268–9274.

[4] For reviews on water oxidation catalysts: a) X. Sala, I. Romero, M. Rodríguez, L. Escriche, A. Llobet, *Angew. Chem.* **2009**, *121*, 2882–2893; *Angew. Chem. Int. Ed.* **2009**, *48*, 2842–2852; b) H. Yamazaki, A. Shouji, M. Kajita, M. Yagi, *Coord. Chem. Rev.* **2010**, *254*, 2483–2491.

[5] For reviews on heterogeneous water-splitting catalysts see: a) X. Chen, S. Shen, L. Guo, S. S. Mao, *Chem. Rev.* **2010**, *110*, 6503–6570; b) A. Kudo, Y. Miseki, *Chem. Soc. Rev.* **2009**, *38*, 253–278; c) F. E. Osterloh, *Chem. Mater.* **2008**, *20*, 35–54; d) K. Maeda, K. Domen, *J. Phys. Chem. C* **2007**, *111*, 7851–7861.

[6] S. W. Gersten, G. J. Samuels, T. J. Meyer, *J. Am. Chem. Soc.* **1982**, *104*, 4029–4030.

[7] a) M. Yagi, A. Syouji, S. Yamada, M. Komi, H. Yamazaki, S. Tajima, *Photochem. Photobiol. Sci.* **2009**, *8*, 139; b) N. D. McDaniel, F. J. Coughlin, L. L. Tinker, S. Bernhard, *J. Am. Chem. Soc.* **2008**, *130*, 210–217; c) R. H. Crabtree, *Chem. Rev.* **2012**, *112*, 1536–1554.

[8] a) J. D. Blakemore, N. D. Schley, D. Balcells, J. F. Hull, G. W. Olack, C. D. Incarvito, O. Eisenstein, G. W. Brudvig. R. H. Crabtree, *J. Am. Chem. Soc.* **2010**, *132*, 16017–16029; b) J. F. Hull, D. Balcells, J. D. Blakemore, C. D. Incarvito, O. Eisenstein, G. W. Brudvig, R. H. Crabtree, *J. Am. Chem. Soc.* **2009**, *131*, 8730–8731.

[9] A. Savini, G. Bellachioma, G. Ciancaleoni, C. Zuccaccia, D. Zuccaccia, A. Macchioni, *Chem. Commun.* **2010**, *46*, 9218–9219.

[10] R. Lalrempuia, N. D. McDaniel, H. Müller-Bunz, S. Bernhard, M. Albrecht, *Angew. Chem.* **2010**, *122*, 9959–9962; *Angew. Chem. Int. Ed.* **2010**, *49*, 9765–9768.

[11] W. I. Dzik, S. E. Calvo, J. N. H. Reek, M. Lutz, M. A. Ciriano, C. Tejel, D. G. H. Hetterscheid, B. de Bruin, *Organometallics* **2011**, *30*, 372–374.

[12] D. G. H. Hetterscheid, J. N. H. Reek, *Chem. Commun.* **2011**, *47*, 2712–2714.

[13] T. P. Brewster, J. D. Blakemore, N. D. Schley, C. D. Incarvito, N. Hazari, G. W. Brudvig, R. H. Crabtree, *Organometallics* **2011**, *30*, 965–973.

[14] A. Savini, P. Belanzoni, G. Bellachioma, C. Zuccaccia, D. Zuccaccia, A, Macchioni, *Green Chem.* **2011**, *13*, 3360–3374.

[15] a) L. Tong, L. Duan, Y. Xu, T. Privalov, L. Sun, *Angew. Chem.* **2011**, *123*, 465–469; *Angew. Chem. Int. Ed.* **2011**, *50*, 445–449; b) L. Duan, Y. Xu, L. Tong, L. Sun, *ChemSusChem* **2011**, *4*, 238–244; c) Y. Xu, A. Fischer, L. Duan, L. Tong, E. Gabrielsson, B. Åkermark, L. Sun, *Angew. Chem.* **2010**, *122*, 9118–9121; *Angew. Chem. Int. Ed.* **2010**, *49*, 8934–8937; d) L. Duan, Y. Xu, M. Gorlov, L. Tong, S. Andersson, L. Sun, *Chem. Eur. J.* **2010**, *16*, 4659–4668; e) L. Duan, Y. Xu, P. Zhang, M. Wang, L. Sun, *Inorg. Chem.* **2010**, *49*, 209–215.

[16] M. D. Kärkäs, E. V. Johnston, E. A. Karlsson, B.-L. Lee, T. Åkermark, M. Shariatgorji, L. Ilag, Ö. Hansson, J.-E. Bäckvall, B. Åkermark, *Chem. Eur. J.* **2011**, *17*, 7953–7959.

[17] S. Roeser, P. Farras, F. Bozoglian, M. Martinez-Belmonte, J. Benet-Buchholz, A. Llobet, *ChemSusChem* **2011**, *4*, 153.

[18] See for example: a) A. Harriman, I. J. Pickering, J. M. Thomas, P. A. Christensen, *J. Chem. Soc. Faraday Trans. 1* **1988**, *84*, 2795–2806; b) R. Nakamura, H. Frei, *J. Am. Chem. Soc.* **2006**, *128*, 10668–10669; c) T. Nakagawa, N. S. Bjorge, R. W. Murray, *J. Am. Chem. Soc.* **2009**, *131*, 15578–15579; d) M. Hara, T. E. Mallouk, *Chem. Commun.* **2000**, 1903–1904; e) S. D. Tilley, M. Cornuz, K. Sivula, M. Grätzel, *Angew. Chem.* **2010**, *122*, 6549–6552; *Angew. Chem. Int. Ed.* **2010**, *49*, 6405–6408; f) S. J. Kwon, F.-R. F. Fan, A. J. Bard, *J. Am. Chem. Soc.* **2010**, *132*, 13165–13167; g) P. G. Hoertz, Y. I. Kim, W. J. Youngblood, T. E. Mallouk, *J. Phys. Chem. B* **2007**, *111*, 6845–6856; h) M. Yagi, E. Tomita, T. Kuwabara, *J. Electroanal. Chem.* **2005**, *579*, 83–88; i) G. S. Nahor, P. Hapiot, P. Neta, A. Harriman, *J. Phys. Chem.* **1991**, *95*, 616–621.

[19] D. B. Grotjahn, D. B. Brown, J. K. Martin, D. C. Marelius, M.-C. Abadjian, H. N. Tran, G. Kalyuzhny, K. S. Vecchio, Z. G. Specht, S. A. Cortes-Llamas, V. Miranda-Soto, C. van Niekerk, C. E. Moore, A. L. Rheingold, *J. Am. Chem. Soc.* **2011**, *133*, 19024–19027.

[20] N. D. Schley, J. D. Blakemore, N. K. Subbaiyan, C. D. Incarvito, F. D'Souza, R. H. Crabtree, G. W. Brudvig, *J. Am. Chem. Soc.* **2011**, *133*, 10473–10481.

[21] D. Hong, M. Murakami, Y. Yamada, S. Fukuzumi, *Energy Environ. Sci.* **2012**, *5*, 5708–5716.

[22] N. Marquet, F. Gärtner, S. Losse, M.-M. Pohl, H. Junge, M. Beller, *ChemSusChem* **2011**, *4*, 1598–1600.

[23] F. Gärtner, S. Denurra, S. Losse, A. Neubauer, A. Boddien, A. Gopinathan, A. Spannenberg, H. Junge, S. Lochbrunner, M. Blug, S. Hoch, J. Busse, S. Gladiali, M. Beller, *Chem. Eur. J.* **2012**, *18*, 3220–3225.

[24] M. S. Lowry, W. R. Hudson, R. A. Pascal, Jr., S. Bernhard, *J. Am. Chem. Soc.* **2004**, *126*, 14129–14135.

[25] For details on the experimental set-up see: a) B. Loges, H. Junge, B. Spilker, C. Fischer, M. Beller, *Chem. Ing. Tech.* **2007**, *79*, 741–753; b) A. Boddien, B. Loges, H. Junge, M. Beller, *ChemSusChem* **2008**, *1*, 751–758.

[26] C. Scheeren, F. Maasarani, A. Hijazi, J.-P. Djukic, M. Pfeffer, *Organometallics* **2007**, *26*, 3336–3345.

[27] B. Schmid, F. O. Garces, R. J. Watts, *Inorg. Chem.* **1994**, *33*, 9–14.

[28] CCDC-866799 contains the supplementary crystallographic data for this paper. These data can be obtained free of charge from The Cambridge Crystallographic Data Centre via www.ccdc.cam.ac.uk/data_request/cif.

[29] Although compound **5** has been already mentioned as an intermediate in our previous publication (see ref. [22]), no analytical data have been provided so far.

[30] D. Lahiri, V. Subramanian, B. A. Bunker, P. V. Kamat, *J. Chem. Phys.* **2006**, *124*, 204720-1-7.

[31] A. Minguzzi, C. Locatelli, G. Cappelletti, M. Scavini, A. Vertova, P. F. Ghigna, S. Rondinini, *J. Phys. Chem. A* **2012**, *116*, 6497–6504.

[32] a) E. Bus, D. E. Ramaker, J. A. van Bokhoven, *J. Am. Chem. Soc.* **2007**, *129*, 8094–8102; b) Y. Akdogan, C. Vogt, M. Bauer, H. Bertagnolli, L. Giurgiu, E. Roduner, *Phys. Chem. Chem. Phys.* **2008**, *10*, 2952–2963; c) N. Guo, B. R. Fingland, W. D. Williams, V. F. Kispersky, J. Jelic, W. N. Delgass, F. H. Ribeiro, R. J. Meyer, J. T. Miller, *Phys. Chem. Chem. Phys.* **2010**, *12*, 5678–5693.

[33] A. A. Bolzan, C. Fong, B. J. Kennedy, C. J. Howard, *Acta Crystallogr. B* **1997**, *53*, 373–380.

[34] a) J. Weitkamp, *Handbook of Porous Solids,* (Eds.: F. Janowski, D. Enke; F. Schüth, K. S. W. Sing), Wiley-VCH, *3*, **2002**, 1432–1434; b) S. Wohlrab, A. Janz, M.-M. Pohl, S. Kreft, D. Enke, A. Köckritz, A. Martin, B. Lücke, *Stud. Surf. Sci. Catal.* **2010**, *175*, 315–319.

[35] a) C. T. Kresge, M. E. Leonowicz, W. J. Roth, J. C. Vartuli, J. S. Beck, *Nature* **1992**, *359*, 710–712; b) J. S. Beck, J. C. Vartuli, W. J. Roth, M. E. Leonowicz, C. T. Kresge, K. D. Schmitt, C. T. D. Chu, D. H. Olson, E. W. Sheppard, S. B. McCullen, J. B. Higgins, J. L. Schlenker, *J. Am. Chem. Soc.* **1992**, *114*, 10834–10843.

[36] a) F. Schüth, A. Wingen, J. Sauer, *Microporous Mesoporous Mater.* **2001**, *44–45*, 465–476; b) A. Taguchi, F. Schüth, *Microporous Mesoporous Mater.* **2005**, *77*, 1–45.

Received: April 28, 2012

Ir walks a fine line: Molecularly defined Ir complexes and IrO_2 nanoparticles have been applied in the water oxidation reaction with cerium ammonium nitrate (CAN) as oxidant and compared (see scheme). The conversion of the first to the latter has been investigated by means of XANES, EXAFS, and STEM.

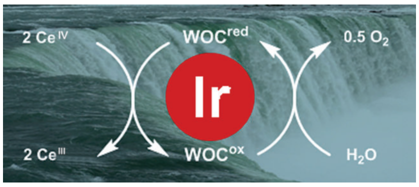

Iridium

H. Junge, N. Marquet, A. Kammer, S. Denurra, M. Bauer, S. Wohlrab, F. Gärtner, M.-M. Pohl, A. Spannenberg, S. Gladiali, M. Beller** .... ■■■■–■■■■

Water Oxidation with Molecularly Defined Iridium Complexes: Insights into Homogeneous Versus Heterogeneous Catalysis

---

Water oxidation…
…is a significant and challenging goal. Succesfully applied molecularly defined Ir complexes are thought to be converted into Ir-oxo nanoparticles that may also act as catalysts. Thus, the iridium performs "tightrope-walking" between homogeneous and heterogeneous catalysis. New insights have been revealed by XANES, EXAFS, and STEM investigations. For more details, see the Full Paper by M. Beller et al. on Page ■■ ff.